PHYSICAL REVIEW B VOLUME 11, NUMBER 10 15 MAY 1975

Dispersion of nonlinear optical susceptibilities of InAs, InSb, and GaAs in the visible region

D. Bethune, A. J. Schmidt, and Y. R. Shen

Department of Physics, University of California, and Inorganic Materials Research Division, Lawrence Berkeley Laboratory, Berkeley, California 94720

(Received 29 January 1975)

We have measured the dispersion of $|\chi^{(2)}(2\omega)|$ for the III-V semiconductors InAs, InSb, and GaAs at 80 and 300 K, with $\hbar\omega$ between 2.0 and 2.7 eV. Large dispersion in $|\chi^{(2)}(2\omega)|$ is found for all three semiconductors, while the results for the two temperatures are similar. We compare the observed structures in $\chi^{(2)}$ with those in $\chi^{(1)}(\omega)$ and $\chi^{(1)}(2\omega)$, and derive Miller's Δ from our experimental values. We also compare our measured $\chi^{(2)}(2\omega)$ with recent theoretical results obtained from empirical pseudopotential calculations.

I. INTRODUCTION

The dispersion of optical nonlinear susceptibilities has always been a subject of great importance in nonlinear optics. It not only predicts how the nonlinear optical effects vary with frequency, but also yields information about the optical properties of the materials. Many researchers are particularly interested in the dispersion of the second-order nonlinear susceptibilities of zinc-blende semiconductors for a number of reasons. Zinc-blende semiconductors have strong nonlinearity, and crystals of large size are readily available. The band structure and the linear optical properties of these semiconductors are fairly well known, and hence the nonlinear susceptibilities can be calculated and compared with the experimental results.

There already exist in the literature several reports on the dispersion of nonlinear susceptibilities of semiconductors. The first measurements by Chang, Ducuing, and Bloembergen[1,2] used nine discrete fundamental frequencies in the range 1.17–2.34 eV, generated by Nd: glass, ruby, and Raman lasers, to study the nonlinear susceptibility $\chi^{(2)}(2\omega)$ for ZnTe, GaAs, InAs, and InSb. Large variations of $\chi^{(2)}(2\omega)$ with ω were reported and partially correlated with optical transitions in the crystals around critical points. Parsons and Chang[3] later used a ruby pumped dye laser, from 1.1 to 1.7 eV, to study $\chi^{(2)}(2\omega)$ vs ω. Their results for GaAs, InAs, and InSb showed some discrepancy with the earlier work. The observed peaks did not all agree with the theoretical predictions. More recently, Lotem *et al.*[4,5] did similar measurements on GaAs, GaSb, and GaP. They showed that their results did agree with the theoretical calculations.

Parsons and Chang[6] also measured the dispersion in $|\chi^{(2)}(2\omega)|$ for the II–VI compounds CdS and CdSe. The result was quite surprising. A broad resonant peak in $\chi^{(2)}(2\omega)$ was seen in CdS at room temperature when ω was about half of the room-temperature "exciton" energy. Haueisen and Mahr[7–9] studied the dispersion of $\chi^{(2)}$ in the region of the first and second 1*s* exciton in CuCl and the C exciton of ZnO at low temperature (20 K). They found pronounced resonances in $\chi^{(2)}$ due to excitons. Second-harmonic generation has also been studied in InSb with a CO_2 laser, the second-harmonic photon energies being near the band edge.[10,11]

In most semiconductors, because of the increasing number of critical points with increasing frequency, we expect to find more structure in $\chi^{(2)}(2\omega)$ at larger ω. This is particularly true when both ω and 2ω are above the band gap. The measurements of $\chi^{(2)}(2\omega)$ of zinc-blende semiconductors have so far been limited to $\hbar\omega < 1.8$ eV. In this paper we report the results of our recent $\chi^{(2)}(2\omega)$ measurements of GaAs, InAs, and InSb with $\hbar\omega$ extended from 2.0 to 2.7 eV.

The theoretical calculation of $\chi^{(2)}(2\omega)$ vs ω is complicated by the complexities of the band structure and the optical transition matrix elements. Some researchers have attempted interpretations of $\chi^{(2)}(2\omega)$ based on simple models[7,9,12] while others have based their interpretations on simplified band-structure calculations.[5,11,13–23] Chang *et al.*[1,2] approximated $\chi^{(2)}(2\omega)$ as a linear combination of the linear susceptibilities, $\chi^{(1)}(\omega)$ and $\chi^{(1)}(2\omega)$. Miller[24] suggested the relation $\chi^{(2)}_{ijk}(2\omega) = \Delta_{ijk}\chi^{(1)}_{ii}(2\omega)\chi^{(1)}_{jj}(\omega)\chi^{(1)}_{kk}(\omega)$, where he assumed Δ_{ijk} to be constant, or slowly varying with ω. In the case of a real solid with dispersion and absorption, however, Δ_{ijk} should in general be a complicated function of ω. Parsons and Chang[3] and Lotem *et al.*[4] have indeed found variation of Δ_{ijk} with ω in their experimental results. In this paper, we shall compare the structure in our measured $\chi^{(2)}(2\omega)$ with those in $\chi^{(1)}(\omega)$ and $\chi^{(1)}(2\omega)$, and then deduce $\Delta_{ijk}(\omega)$. We shall also compare our measured $\chi^{(2)}(2\omega)$ with the theoretical results obtained by empirical pseudopotential calculations.

In Sec. II, we first give a brief review of the theory of $\chi^{(2)}(2\omega)$. We then describe the experimental procedure in Sec. III. We present the re-

sults in Sec. IV and, finally, compare the measured results with theory in Sec. V.

II. THEORY OF $\chi^{(2)}(2\omega)$

Theoretical calculations on $\chi^{(2)}(2\omega)$ can be grouped into attempts to find numerical values of $\chi^{(2)}(2\omega)$ at low frequencies (ω is much smaller than the band gap but larger than the lattice vibrational frequencies)[12-21] and attempts to derive the dispersion of $\chi^{(2)}(2\omega)$.[22,23,25] In the former case, bond models have been used with a reasonably high degree of success.[17-21] In the latter case, especially when ω and 2ω are above the band gap, the dispersion of $\chi^{(2)}(2\omega)$ depends on the details of the band structure.

The basic equation for $\chi^{(2)}(2\omega)$ derived from second-order perturbation calculation for zinc-blende semiconductors is[22,23,25]

$$\chi_{14}^{(2)}(2\omega)=-\frac{\sqrt{3}e^3}{4m^3\omega^3}\int_{\text{B.z.}} d^3k \sum_{c,c',v} p_{vc}p_{cc'}p_{c'v}\{(E_{cv}-2\hbar\omega)^{-1}(E_{c'v}-\hbar\omega)^{-1}+(E_{cv}-\hbar\omega)^{-1}(E_{c'v}+\hbar\omega)^{-1}+(E_{cv}+\hbar\omega)^{-1}(E_{c'v}+2\hbar\omega)^{-1}\}, \quad (1)$$

where $E_{cv}(\vec{k})$ is the energy separation between the conduction band c and the valence band v at $\vec{k}$ in the Brillouin zone and p_{vc} is the corresponding momentum matrix element along the [111] direction. Chang *et al.*[1] rearranged Eq. (1) into the form

$$\chi_{14}^{(2)}(2\omega)=A\int_{\text{Bz}} d^3k \sum_{c,v}\left(\frac{Q_{cv}^{(1)}(\vec{k})}{\omega^2-\omega_{cv}^2}+\frac{Q_{cv}^{(2)}(\vec{k})}{4\omega^2-\omega_{cv}^2}\right), \quad (2)$$

where A is a constant. If both $p_{cv}(\vec{k})$ and $Q_{cv}^{(1),(2)}(\vec{k})$ are assumed to be independent of ω and $\vec{k}$, the $\chi_{14}^{(2)}(2\omega)$ could be written as a linear combination of the linear susceptibilities $\chi^{(1)}(\omega)$ and $\chi^{(1)}(2\omega)$. The structure in the dispersions of $\chi^{(1)}(\omega)$ and $\chi^{(1)}(2\omega)$ would be reflected in $\chi^{(2)}(2\omega)$.

However, in Eq. (1), we notice that there are two types of resonances, i.e., single resonances, when $\hbar\omega=E_{cv}$ or $2\hbar\omega=E_{cv}$ and double resonances when $\hbar\omega=E_{cv}$ and $2\hbar\omega=E_{c'v}$ at the same $\vec{k}$ point. In the latter case, $Q_{cv}^{(1)}(\vec{k})$ or $Q_{cv}^{(2)}(\vec{k})$ in Eq. (2) would have a singularity, and hence the assumption that they are independent of ω and $\vec{k}$ breaks down.

Bell[23] used a simplified three-band model to calculate $\chi_{14}^{(2)}(2\omega)$ for ω between 0.05 and 2.0 eV. He assumed constant momentum matrix elements and anticipated the structure in $\chi^{(2)}(2\omega)$ to arise from critical-point transitions at Γ and along Λ in the Brillouin zone. His calculations are in fair agreement with the available experimental results.[1-4] However, he has probably given too much weight to the Γ-point transitions since it is well known that the density of states near Γ is small.

Recently, Fong and Shen[25] have calculated $\chi_{14}^{(2)}(2\omega)$ from Eq. (1) with four lowest conduction bands and four highest valence bands. The wavefunctions and energies of the band states were obtained from the empirical pseudopotential method. Such a method has been very successful in reproducing the observed linear optical spectra of zinc-blende semiconductors.[26] We shall compare their calculations with our experimental results on $\chi^{(2)}(2\omega)$ in Sec. V.

III. EXPERIMENTAL ARRANGEMENT

A. Experimental setup

We used a flash-pumped dye laser as the source of the fundamental beam in our experiments. Its output was well polarized, 1 μsec long, with a peak power of 1–10 kW, a linewidth of about 10 Å, and a beam cross section of about 7 mm^2. With different dyes (Table I), the laser had a tuning range from 2.0 to 2.7 eV. A pulse repetition rate of 1–2 pps was used. The overall experimental setup is shown in Fig. 1. A beam splitter was used to separate the laser beam into two parts. One beam was directed through a quartz crystal 2 mm thick, which generated second harmonics used for normalization against possible laser fluctuations.[27,28] The other beam was used to generate second harmonics either by reflection from a sample or by transmission through a similar quartz crystal (dotted path in Fig. 1). The second-harmonic signal from this second quartz crystal was needed for calibration of the nonlinear susceptibility of the sample, as we shall see later. A 15-cm focal length lens was used to focus the laser beams on the sample and on the quartz plates. The second-harmonic signals from the two beams then went through a filter and two monochromators in tandem simultaneously and fell on two separate

TABLE I. Dyes and tuning ranges.

Dye	Solvent	Conc. (mg/liter)	Tuning range
7-Diethylamino 4-Methylcoumarin	Ethanol	100	4500–4950 Å
Coumarin 30	Ethanol	30	4900–5200 Å
Coumarin 6	Ethanol	25	5200–5600 Å
Rhodamine 6G	H_2O+HFIP 2:1	60	5600–6100 Å
Rhodamine 6G	Ethanol	60	5700–6300 Å

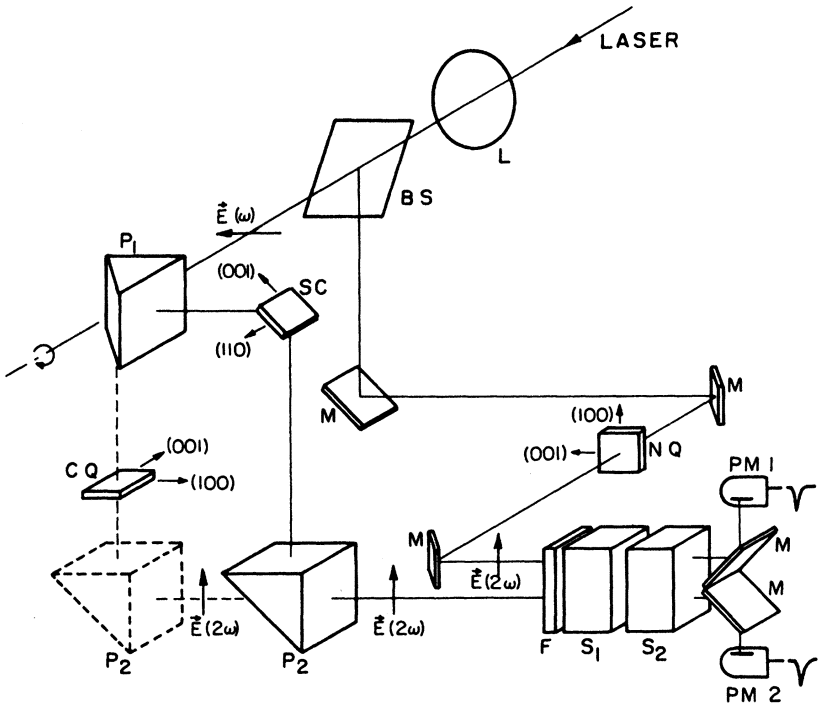

FIG. 1. Experimental setup: L—lens; BS—beam splitter; M—mirrors; P_1—90° prims; P_2—90° quartz prism; SC—semiconductor sample; CQ—calibration quartz crystal; NQ—normalization quartz crystal; F—filter (1 cm cell of $CoSO_4$ saturated in H_2O for $\lambda < 5200$ Å; Corning 7–54 for $\lambda > 5200$ Å); S_1 and S_2—1/4 meter spectrometers in tandem; PM_1 and PM_2—RCA 1P28 photomultipliers.

photomultipliers. The two output pulses were sent into two gated electronic integrators and then digitized for display. Each point in the data was obtained by averaging the results over 100–200 laser shots.

The measurements were done with the sample mounted on a cold finger in a simple Dewar at 300 and at 80 K. Two samples of GaAs with different orientations were measured, one with a cleaved (110) face and the other with a polished (111) face. In the cases of InAs and InSb, only cleaved samples with (110) face were used.

B. Sample preparation

To check the orientation of the samples and the quality of their surfaces, the second-harmonic intensity polarized in the plane of incidence was measured while rotating the sample about its surface normal.

The expected variation with angle can be derived from Bloembergen and Pershan's[29] work. Let $\hat{z}$ be the normal to the crystal face, and the $x-z$ plane be the plane of incidence. The incident light is polarized along y, and the angle of incidence is 45°. For the (111) crystal face, the induced nonlinear polarization is

$$\vec{P}_{NL}(111)=\frac{\chi_{14}E_c^2}{2}\sqrt{\frac{2}{3}}\begin{pmatrix}-\cos 3\phi\\ \sin 3\phi\\ -1/\sqrt{2}\end{pmatrix}, \tag{3}$$

where ϕ is the angle of rotation about the z axis, with $\phi = 0$ corresponding to the (100) axis lying in the plane of incidence and E_c is the electric field inside the crystal. Then, the variation of the reflected second-harmonic intensity with ϕ is

$$I_{\parallel}^{(111)}(\phi)\propto |2\epsilon(2\omega)-1|\cos^2 3\phi - \sqrt{2}\,\mathrm{Re}\,[2\epsilon(2\omega)-1]^{1/2}\cos 3\phi+\tfrac{1}{2}, \tag{4}$$

where $\epsilon(\omega)$ is the linear dielectric constant. For the (110) crystal face, we have

$$\vec{P}_{NL}(110)=\frac{\chi_{14}E_c^2}{2}\begin{pmatrix}\sin\phi(\sin^2\phi-2\cos^2\phi)\\ -3\cos\phi\sin^2\phi\\ 0\end{pmatrix}, \tag{5}$$

$$I_{\parallel}^{(110)}(\phi)\propto \sin^2\phi\,(\sin^2\phi-2\cos^2\phi)^2, \tag{6}$$

where $\phi = 0$ when the [001] axis is parallel to $\hat{y}$. The results of our measurements, as shown in Figs. 2 and 3 for the cleaved (110) and the polished (111) GaAs samples, respectively, agree well with the theoretical predictions.

The quartz crystals used were cut with the optical axis parallel to the surface. Both the incident laser beam and the generated second harmonic were polarized perpendicular to the optical axis. According to Ref. 29, the second-harmonic output from the quartz is proportional to

$$|E_T^{2\omega}|^2=\left|4\pi\chi_{11}^{(2)}\left(\frac{2E_0}{1+n_1}\right)^2\right|^2\left(\frac{1+n_1}{n_2^2-n_1^2}\right)^2 \times\langle\sin^2\tfrac{1}{2}(2k_\omega-k_{2\omega})d\rangle, \tag{7}$$

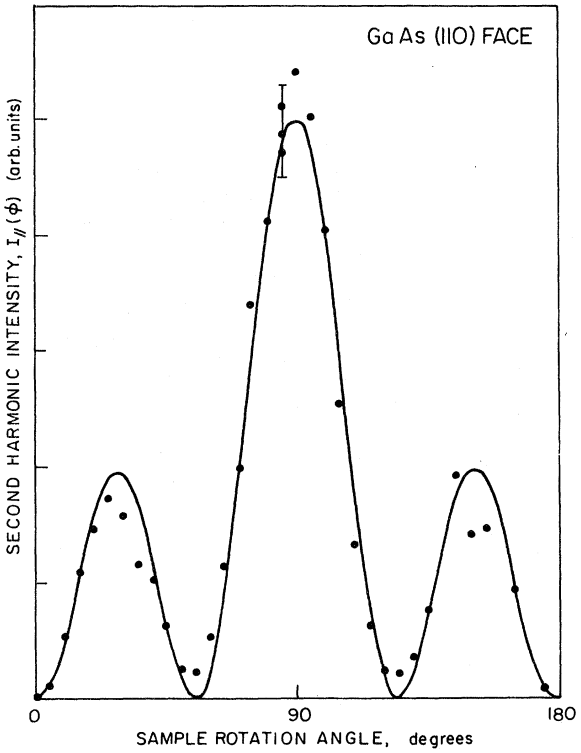

FIG. 2. Variation of second-harmonic intensity polarized parallel to the plane of incidence with ϕ, the angle of rotation about the crystal face normal, for a cleaved (110) face of GaAs. The solid curve is the theoretical variation from Eq. (6), normalized to the experimental maximum.

where E_0 is the incident laser field, n_1 and n_2 are the ordinary indices of refraction of ω and 2ω, respectively. k_ω is the magnitude of the wave vector at ω and d is the thickness of the quartz plate. The brackets $\langle\rangle$ indicate averaging of the "Maker fringe" factor[30] over the laser bandwidth and random jitter of the laser frequency. In our case, the dye laser gave $\langle \sin^2\psi\rangle \simeq \frac{1}{2}$.

C. Experimental procedure

We first measured the ratio of the second-harmonic outputs from the two quartz plates. Then, we switched the beam from the calibration quartz to the sample and measured the ratio of the second-harmonic outputs from the sample and from the normalization quartz. At each laser frequency, the results were averaged over 100 to 200 laser pulses. We also took the precaution of subtracting the residual noise from the total output of each channel before taking the ratio of the two outputs. The noise level (which was generally less than a few percent of the signal) was obtained by measuring the output with a filter which transmitted the laser but blocked the second harmonics in front of the double monochromators.

IV. DATA-PROCESSING PROCEDURE

The expression given in Ref. 29 for the second-harmonic field generated in reflection from a semiconductor can be reduced for 45° incidence to the form

$$E_{R\,/\!/}^{2\omega} = \frac{\sqrt{32}\pi\,(f_2 P_x^{\mathrm{NL}} - P_x^{\mathrm{NL}})}{(f_1+f_2)\,(\epsilon_2+f_2)}\ , \tag{8}$$

where $f_1 = [2\epsilon(\omega)-1]^{1/2}$ and $f_2 = [2\epsilon(2\omega)-1]^{1/2}$. From Eqs. (3) and (5) with $\phi = 90°$ for the (110) crystal face and $\phi = 60°$ for the (111) crystal face we find, respectively,

$$E_{R/\!/}^{(2\omega)}(110) = R(110)\chi_{14}^{(2)}E_0^2\ , \tag{9}$$

$$E_{R/\!/}^{(2\omega)}(111) = R(111)\chi_{14}^{(2)}E_0^2, \tag{10}$$

where

$$R(110) = \frac{\sqrt{8}\pi[2/(1+f_1)]^2 f_2}{(f_1+f_2)(f_2+\epsilon_2)}$$

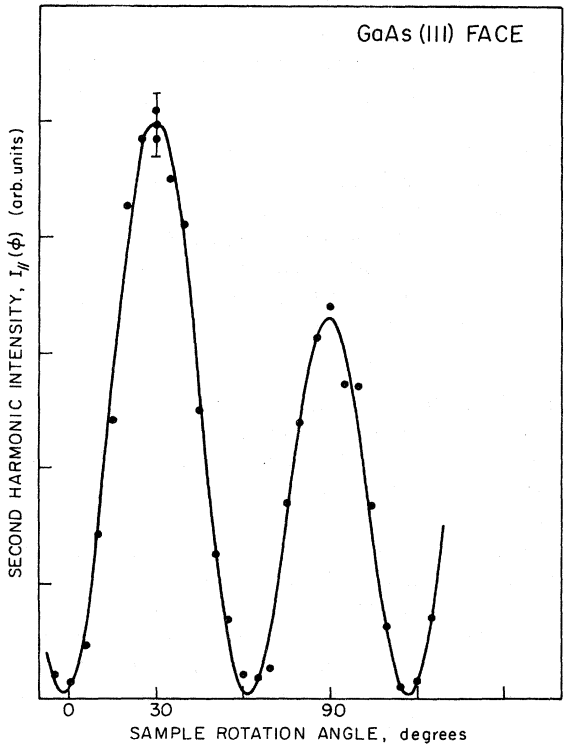

FIG. 3. Variation of second-harmonic intensity polarized parallel to the plane of incidence with ϕ, the rotation angle about the crystal face normal, for a polished (111) face of GaAs. The solid curve is the theoretical variation from Eq. (4), normalized to the experimental maximum.

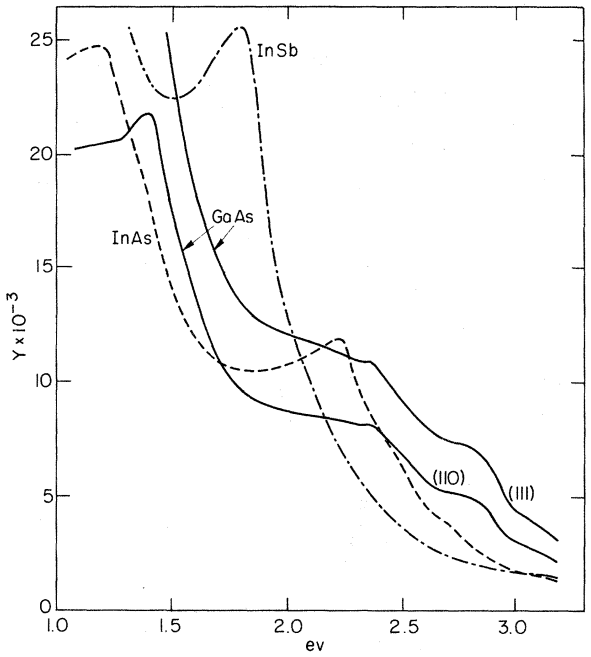

FIG. 4. Values of the linear correction factor Y defined in Eq. (13) of text.

and

$$R(111)=\sqrt{8}\pi\left(\frac{2}{1+f_1}\right)^2\sqrt{\tfrac{2}{3}}f_2+\frac{1/\sqrt{3}}{(f_1+f_2)(f_2+\epsilon_2)}\,.$$

The second-harmonic field from the quartz plates can be written [following Eq. (7)]

$$E_T^{(2\omega)}=\frac{1}{\sqrt{2}}T\chi_{11}^{(2)}E_0^2\,, \tag{11}$$

with

$$T=\frac{16\pi}{(n_2^2-n_1^2)(1+n_1)}\,.$$

Let γ be the ratio of the second-harmonic intensities from the calibration quartz and the normalization quartz. Then, the ratio of the second-harmonic intensity from the semiconductor ($I_{SC}^{2\omega}$) to the second-harmonic intensity from the calibration quartz ($I_{CQ}^{2\omega}$) is

$$\frac{I_{SC}^{2\omega}}{I_{CQ}^{2\omega}}=\frac{|R\chi_{14}^{(2)}|^2}{\frac{1}{2}|T\chi_{11}^{(2)}|^2}=\frac{I_{SC}^{2\omega}}{\gamma I_{RQ}^{2\omega}}\,: \tag{12}$$

where $I_{RQ}^{2\omega}$ is the second-harmonic intensity generated from the normalization quartz plate. Therefore, we have

$$|\chi_{14}^{(2)}|/|\chi_{11}^{(2)}|=Y\sqrt{I_{SC}^{2\omega}/2\gamma I_{RQ}^{2\omega}}\,, \tag{13}$$

where $Y=|T|/|R|$, as defined by Parsons and Chang.[3] To compute Y, we used the linear dielectric constants given in Ref. 31 for the semiconductors at room temperature, and the indices of refraction for quartz given in Ref. 32. In Fig. 4, Y is plotted for the three crystals we have measured. Note that Y also depends on the crystal orientation. We also realize that uncertainty in the linear dielectric constants will affect Y, and lead to uncertainty in the values of nonlinear susceptibilities. The numerical value for $\chi_{11}^{(2)}(2\omega)$ of quartz is given in Ref. 33 as 1.2×10^{-9} esu.

V. RESULTS

Figures 5–7 show the experimental results of $|\chi_{14}^{(2)}(2\omega)|$ for the three compounds normalized

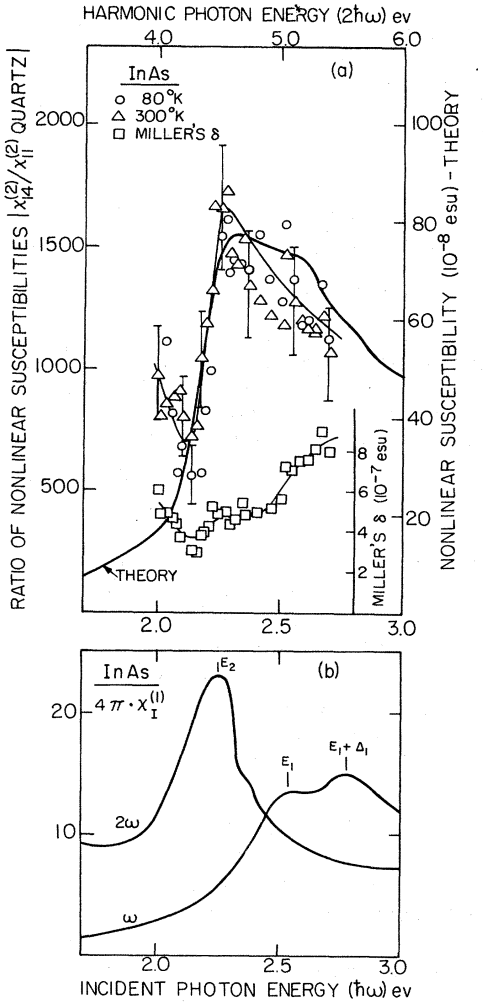

FIG. 5. (a) Experimental values of ratio of nonlinear susceptibilities $|\chi_{14}^{(2)}(\text{InAs})/\chi_{11}^{(2)}(\text{quartz})|$ at 80 and 300 K. The light curve is a rough fit to the data, and the heavier curve is the theoretical calculation of Fong and Shen (Ref. 25). Also shown are the values of Miller's Δ derived from the experimental data and the linear constants. (b) The imaginary dielectric constants $\epsilon_I(\omega)=4\pi\chi_I^{(1)}(\omega)$ and $\epsilon_I(2\omega)=4\pi\chi_I^{(1)}(2\omega)$ for InAs. The features corresponding to the E_1 and E_2 peaks are indicated.

against $|\chi_{11}^{(2)}(2\omega)|$ of quartz. They are compared with the theoretical curves of $|\chi_{14}^{(2)}(2\omega)|$ calculated by Fong and Shen[25] using the empirical pseudopotential method. We also show in the figures the imaginary parts of the dielectric constants $\epsilon_2(\omega)$ and $\epsilon_2(2\omega)$ deduced from linear reflectivity measurements,[31] and the Miller $\Delta(\omega)$ defined by $\Delta = |\chi_{14}^{(2)}(2\omega)|/|\chi^{(1)}(\omega)|^2|\chi^{(1)}(2\omega)|$. In the frequency range we have studied, the most prominent features in $\epsilon_2(\omega)$ and $\epsilon_2(2\omega)$ for all the three compounds are the E_1 and $E_1+\Delta_1$ spin-orbit split peaks and the E_2 peak, following the notations of Cardona.[34] The E_1 and $E_1+\Delta_1$ peaks come from transitions between the top spin-orbit split valence bands and the bottom conduction band along the Λ symmetry direction in the Brillouin zone (see Fig. 8 for a typical band structure for III-V compounds.)[26,35] The E_2 peak is due to transitions between the two top valence bands and the two bottom conduction bands in the general region around X, Σ, and Δ, as indicated in Fig. 8. In all the three compounds, we have found that the measured

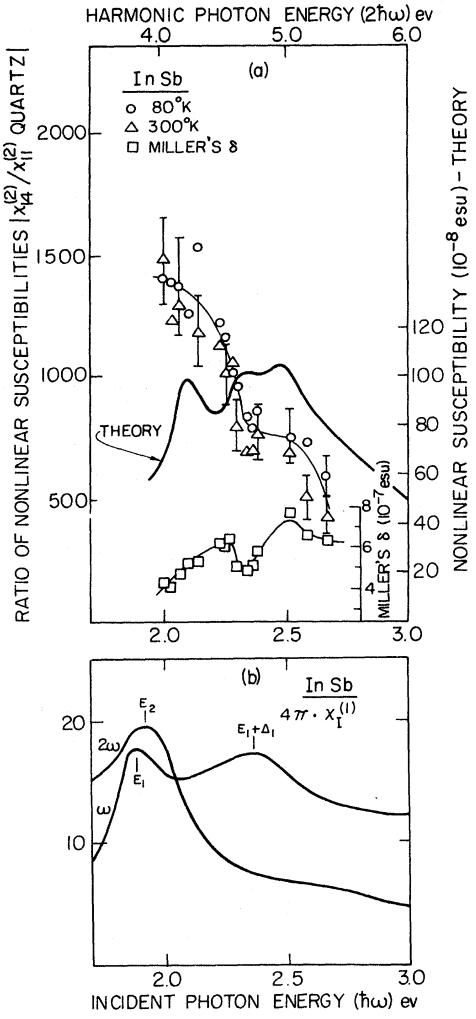

FIG. 6. (a) Experimental values of ratio of nonlinear susceptibilities $|\chi_{14}^{(2)}(\text{InSb})/\chi_{11}^{(2)}(\text{quartz})|$ at 80 and 300 K. The light curve is a rough fit to the data, and the heavier curve is the theoretical calculation of Fong and Shen (Ref. 25). Also shown are the values of Miller's Δ derived from the experimental data and the linear constants. (b) The imaginary dielectric constants $\epsilon_I(\omega) = 4\pi\chi_I^{(1)}(\omega)$ and $\epsilon_I(2\omega) = 4\pi\chi_I^{(1)}(2\omega)$ for InSb. The features corresponding to the E_1 and E_2 peaks are indicated.

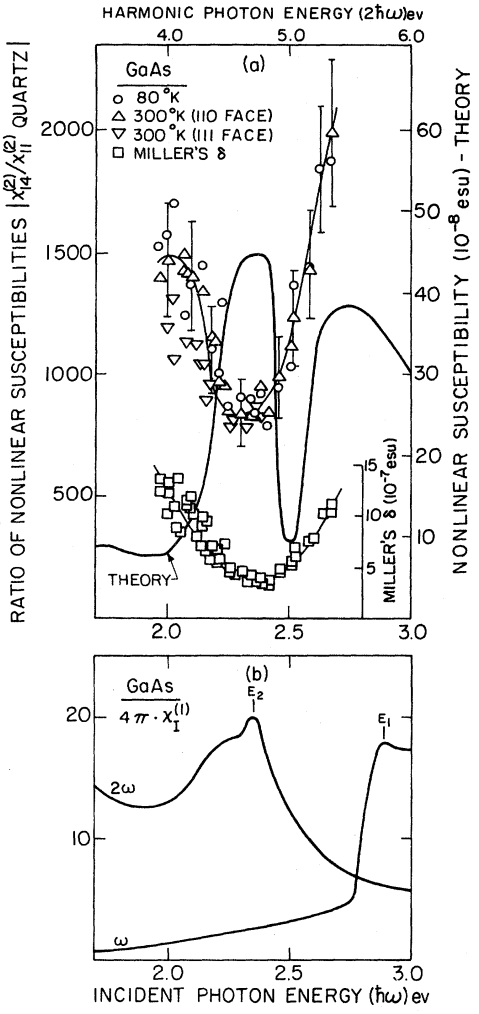

FIG. 7. (a) Experimental values of ratio of nonlinear susceptibilities $|\chi_{14}^{(2)}(\text{GaAs})/\chi_{11}^{(2)}(\text{quartz})|$ at 80 and 300 K. The light curve is a rough fit to the data, and the heavier curve is the theoretical calculation of Fong and Shen (Ref. 25). Also shown are the values of Miller's Δ derived from the experimental data and the linear constants. (b) The imaginary dielectric constants $\epsilon_I(\omega) = 4\pi\chi_I^{(1)}(\omega)$ and $\epsilon_I(2\omega) = 4\pi\chi_I^{(1)}(2\omega)$ for GaAs. The features corresponding to the E_1 and E_2 peaks are indicated.

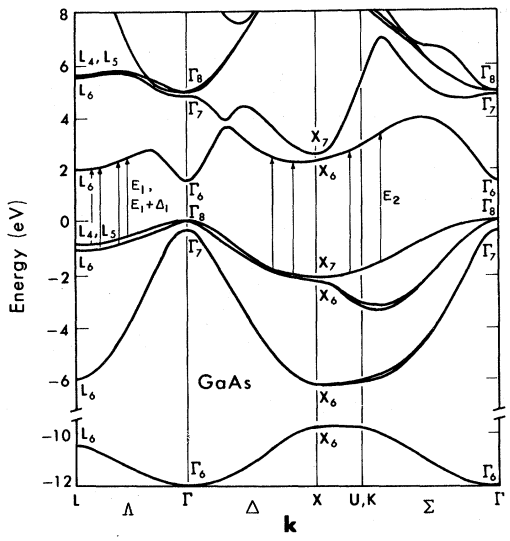

FIG. 8. A typical band structure computed by the empirical pseudopotential method (Ref. 26). The transitions corresponding to the E_1 and E_2 peaks are indicated.

$|\chi_{14}^{(2)}(2\omega)|$ at 80 and at 300 K are not significantly different.

A. InAs

The measured nonlinear susceptibility $|\chi_{14}^{(2)}(2\omega)|$ shows a clear peak at about 2.28 eV with a shoulder at ~2.5 eV. It falls off more sharply on the low-energy side, and begins to rise somewhat at 2 eV.

We have seen in Eq. (2) that the structures in $|\chi_{14}^{(2)}(2\omega)|$ may be related to single resonances of ω in $\epsilon_2(\omega)$ or 2ω in $\epsilon_2(2\omega)$. The positions of the observed structures in $|\chi_{14}^{(2)}(2\omega)|$ of InAs suggest that the peak may correspond to the E_2 peak in $\epsilon_2(2\omega)$ and the shoulder to the E_1 peak in $\epsilon_2(\omega)$. This assignment is confirmed by the theoretical calculation of Ref. 25 which shows good agreement with the shape of the experimental results in Fig. 5. The E_2 peak in InAs comes mainly from transitions between the top valence band and the bottom conduction band around Σ and X in the Brillouin zone.[26,34–36] That the structures in $|\chi_{14}^{(2)}(2\omega)|$ correspond to those in $\epsilon_2(\omega)$ and $\epsilon_2(2\omega)$ is also reflected by the much smoother variation of the Miller Δ[24] with ω. The possible double resonances in $|\chi_{14}^{(2)}(2\omega)|$ do not appear to be important in this case.

B. InSb

In InSb, the measured $|\chi_{14}^{(2)}(2\omega)|$ decreases quite steeply as ω increases from 2.0 eV with a shoulder at 2.4 eV and possibly another one at 2.2 eV. The linear $\epsilon_2(\omega)$ and $\epsilon_2(2\omega)$ at room temperature suggest possible structures in $|\chi_{14}^{(2)}(2\omega)|$ at 1.9 eV arising from the broad E_2 peak in $\epsilon_2(2\omega)$ and the E_1 peak in $\epsilon_2(\omega)$ and 2.4 eV arising from the $E_1+\Delta_1$ peak in $\epsilon_2(\omega)$. The E_2 peak in InSb is due to transitions along Δ from the two top valence bands to the two bottom conduction bands and along Σ from the top valence band to the bottom conduction band.[26,34–36] Despite the overlapping contributions of the E_1 and E_2 peaks around 1.9 eV in $|\chi_{14}^{(2)}(2\omega)|$, this is not a case of double resonance discussed earlier since the transitions responsible for the E_1 and E_2 peaks respectively occur in different regions of the Brillouin zone. Double resonance contributions to $|\chi_{14}^{(2)}(2\omega)|$ do not seem to be important in this case. The 0 K theoretical calculations of Fong and Shen[25] confirm the above general assignment, but the structures of $|\chi_{14}^{(2)}(2\omega)|$ appear to be shifted to the higher energies presumably because of the temperature difference and the relative strengths of the various structures do not agree with the experimental results. The Miller's Δ as a function of ω is again much smoother than $|\chi_{14}^{(2)}(2\omega)|$.

C. GaAs

The $|\chi_{14}^{(2)}(2\omega)|$ data of GaAs show a pronounced peak at 2.1 eV, fall to a deep minimum at 2.35 eV, and then rise steeply again. The peaks in $\epsilon_2(\omega)$ and $\epsilon_2(2\omega)$ of GaAs resemble those of $\chi^{(2)}(2\omega)$ quite closely, except that the corresponding peaks are shifted. They suggest that in $|\chi_{14}^{(2)}(2\omega)|$, one peak should appear at ~2.3 eV arising from the E_2 peak in $\epsilon_2(2\omega)$ and another peak should appear at ~3 eV arising from the E_1 peak in $\epsilon_2(\omega)$. The E_2 peak is due to transitions along Δ from the two top valence bands to the bottom conduction band and along Σ from the top valence band to the bottom conduction band.[26,34–36] The pseudopotential calculations of $|\chi_{14}^{(2)}(2\omega)|$ of Fong and Shen[25] (Fig. 7) show the corresponding peaks at 2.3 and 2.75 eV. Except for a shift of 0.2 eV presumably reflecting a difference in temperature, the theoretical curve is in good agreement with the experimental results. The experimental results were found to be well reproducible and independent of the surface orientation ((111) or (110)) of the sample. Because of the observed shift of the peaks in $|\chi_{14}^{(2)}(2\omega)|$ relative to $\epsilon_2(\omega)$ and $\epsilon_2(2\omega)$, the Miller Δ for GaAs appears to vary strongly with ω in the region we have studied.

VI. DISCUSSION

As discussed in the previous sections, the nonlinear susceptibility $|\chi^{(2)}(2\omega)|$ has resonant structure when either ω or 2ω (or both) approaches resonant peaks in the linear dielectric constant. Thus, in a given frequency range, the spectrum of $|\chi^{(2)}(2\omega)|$ should reveal more structure than the linear optical spectrum. Then, in principle, the former can provide a more critical check on the band structure calculations than the latter. Un-

fortunately, there still exist a number of difficulties in the experimental determination of $|\chi^{(2)}(2\omega)|$.

First, the experimental accuracy in nonlinear optical spectroscopy is still much less than that in linear spectroscopy. Even with the proper normalization scheme designed to eliminate the effect of laser fluctuations, the statistical variation of the results of second-harmonic measurements is large. In our experiments, the results of different runs are reproducible to about 20%. At least part of the error comes from statistical fluctuations of the weak second-harmonic signal. The situation can be greatly improved when single-mode dye lasers with considerably higher power become available.

Second, the high laser intensity on the sample surface may heat up the sample appreciably through absorption. We have found in our experiments that the measured $|\chi^{(2)}(2\omega)|$ with samples at 300 and at 80 K are not noticeably different. This suggests that the laser pulse may have induced a temperature rise of several hundred degrees in the surface layer of the sample. A simple estimate, using the known heat capacity and the calculated 1 μsec diffusion length of the sample and assuming instant thermalization, also gives a temperature increase of several hundred degrees. We therefore expect that the observed peaks may have shifted to lower energies by a few tenths of an eV.[36] Figures 5–7 show that such a shift would indeed improve the agreement between theory and experiment, noticeably in the cases of GaAs and InSb. In order to reduce the temperature rise, one must decrease the laser intensity on the sample, but then in order to have the same second-harmonic signal, one must use a laser beam with higher power and larger cross-sectional area. The high laser intensity may also induce a dense plasma of electrons and holes in the surface layer of the sample. This may lead to changes in linear and nonlinear optical spectra. However, if we assume a carrier lifetime of 10^{-14} sec, then under our experimental conditions, the plasma density is only 10^{17}–$10^{18}/\mathrm{cm}^3$, which should have negligible effect on the optical spectra.

Third, as shown in Eq. (13), the nonlinear susceptibility $|\chi^{(2)}(2\omega)|$ deduced from the measured second-harmonic intensity is proportional to the quantity Y which, in turn, depends on the linear dielectric constants $\epsilon(\omega)$ and $\epsilon(2\omega)$ of the sample through R defined in Eq. (10). An error in ϵ leads to approximately twice the error in Y. Usually, the linear dielectric constant $\epsilon(\omega)$ is deduced from linear reflectivity measurements in a finite frequency range, and the results often depend on how the reflectivity is extrapolated outside the limited frequency range.

The error in ϵ will change the values of $|\chi^{(2)}(2\omega)|$, but may or may not affect the structure in $|\chi^{(2)}(2\omega)|$, appreciably. In Fig. 4, the "Y" values are computed using ϵ deduced from room-temperature measurements.[31] At lower temperatures, the structure in ϵ and the corresponding structure in Y are expected to shift to higher energies with a rate of $\sim 3\times10^{-4}$ eV/K.[35] For InSb and GaAs, the Y curves are quite smooth between 2.0 and 2.7 eV. No appreciable change in the structure of $|\chi^{(2)}(2\omega)|$ at low temperature should be introduced by using the room-temperature Y values to deduce $|\chi^{(2)}(2\omega)|$. For InAs, the room-temperature Y curve has a peak at 2.25 eV which shifts with temperature. This means that the corresponding peak of $|\chi^{(2)}(2\omega)|$ at liquid N_2 temperature in Fig. 5 could be about 0.1 eV higher in energy.

Fourth, we have normalized the measured $|\chi^{(2)}(2\omega)|$ against the nonlinear susceptibility $|\chi_{11}^{(2)}(2\omega)|$ of quartz, assuming that the dispersion of the latter is negligible. This assumption is good in the frequency range we have investigated since the absorption band of quartz starts around 7.5 eV. It, however, becomes a problem if we want to extend the frequency range further into uv. In principle, we can find $|\chi^{(2)}(2\omega)|$ without normalization by calibrating the entire detection system over the frequency range, but such a calibration process is very difficult.

The discrepancies between theory and experiment in Figs. 5–7 may also be due to inaccuracy in the theoretical calculations. In pseudo-potential calculations, the calculated matrix elements are usually much less accurate than the calculated eigenenergies. Consequently, the shapes and strengths of the structure in a calculated spectrum are less reliable than the positions of the structures. We should also remark that the theoretical curves in Figs. 5–7 were obtained without taking into account the frequency dependence of the local field correction. Since the local-field correction factor appears in $|\chi^{(2)}(2\omega)|$ as a triple product of those appearing in $\chi^{(1)}(\omega)$ and $\chi^{(1)}(2\omega)$, it should affect $|\chi^{(2)}(2\omega)|$ much more strongly than $\epsilon(\omega)$ or $\epsilon(2\omega)$. Unfortunately, no reliable model is yet available for even an estimate of the frequency-dependent local-field correction in semiconductors.

A glance at Figs. 5–7 would suggest that for the experimental data to be more meaningful, they should be extended over a larger frequency range. Comparison between theory and experiment could then be made over a number of pronounced structures in the spectrum. Such an experiment requires a relatively high-power laser with a wide tuning range, e.g., from 1 to 3 eV. With the recent advances in dye lasers, this may soon be possible.

VII. CONCLUSION

We have measured $|\chi_{14}^{(2)}(2\omega)|$ for InAs, InSb, and

GaAs at 80 and 300 K with ω extended from 2.0 to 2.7 eV. The accuracy of the measurements is about 20%. There appears to be no obvious difference between results obtained at the two temperatures, presumably because of laser heating of the samples. The experimental data show fair agreement with the theoretical calculations of Fong and Shen,[25] except that the structure in $|\chi_{14}^{(2)}(2\omega)|$ are obviously displaced and the relative strengths of the structures may be different.

The spectrum of $|\chi^{(2)}(2\omega)|$ can, in principle, yield more detailed information about the band structure of a crystal. At present, it is, however, limited by the inaccuracy of the measurements and other difficulties. When improved high-power dye lasers with a wide tuning range become available, the measurements of $|\chi^{(2)}(2\omega)|$ will definitely be easier and more accurate, and their usefulness in probing electronic structures of solids will correspondingly increase.

[1]R. K. Chang, J. Ducuing, and N. Bloembergen, Phys. Rev. Lett. 15, 415 (1965).

[2]N. Bloembergen, R. K. Chang, and J. Ducuing, in *Physics of Quantum Electronics*, edited by P. L. Kelley, B. Lax, and P. E. Tannenwald (McGraw-Hill, New York, 1966), p. 67.

[3]F. G. Parsons and R. K. Chang, Opt. Commun. 3, 173 (1971).

[4]H. Lotem, G. Koren, and Y. Yacoby, Phys. Rev. B 9, 3532 (1974).

[5]H. Lotem and Y. Yacoby, Phys. Rev. B (to be published).

[6]F. G. Parsons, E. Yi-Chen, and R. K. Chang, Phys. Rev. Lett. 27, 1436 (1971).

[7]D. C. Haueisen and H. Mahr, Phys. Rev. Lett. 26, 838 (1971).

[8]D. C. Haueisen, Solid State Commun. 10, 1313 (1972).

[9]D. C. Haueisen and H. Mahr, Phys. Rev. B 8, 734 (1973).

[10]J. J. Wynne, Phys. Rev. Lett. 27, 17 (1971).

[11]S. S. Jha and J. J. Wynne, Phys. Rev. B 5, 4867 (1972).

[12]F. N. H. Robinson, Bell Syst. Tech. J. 46, 913 (1967).

[13]S. S. Jha and N. Bloembergen, Phys. Rev. 171, 891 (1968).

[14]C. Flytzanis and J. Ducuing, Phys. Rev. 178, 1218 (1969).

[15]J. C. Phillips and J. H. Van Vechten, Phys. Rev. 183, 709 (1969).

[16]D. A. Kleinman, Phys. Rev. B 2, 3139 (1970).

[17]C. L. Tang and C. Flytzanis, Phys. Rev. 183, 709 (1969).

[18]D. S. Chemla, Phys. Rev. Lett. 26, 1441 (1971).

[19]B. F. Levine, Phys. Rev. Lett. 22, 787 (1969); Phys. Rev. Lett. 25, 440 (1970).

[20]B. F. Levine, Phys. Rev. B 7, 2600 (1973).

[21]B. F. Levine, Phys. Rev. B 10, 1655 (1974).

[22]P. L. Kelley, J. Phys. Chem. Solids 24, 607 (1963); J. Phys. Chem. Solids 24, 1113 (1963).

[23]M. I. Bell, in *Electronic Density of States*, edited by L. H. Bennett, Natl. Bur. Std. (U.S.) Spec. Publ. No. 323 (U.S. GPO, Washington, D. C., 1971), p. 757; Phys. Rev. B 6, 516 (1972).

[24]R. C. Miller, Appl. Phys. Lett. 5, 17 (1964).

[25]C. Y. Fong and Y. R. Shen, Phys. Rev. B (to be published).

[26]M. L. Cohen and V. Heine, in *Solid State Physics*, edited by H. Ehrenrich, F. Seitz, and D. Turnbull (Academic, New York, 1970), Vol. 24, p. 38.

[27]J. Ducuing and N. Bloembergen, Phys. Rev. Lett. 10, 474 (1963).

[28]J. Ducuing and N. Bloembergen, Phys. Rev. 133, A1493 (1964).

[29]N. Bloembergen and P. S. Pershan, Phys. Rev. 128, 606 (1962).

[30]P. D. Maker, R. W. Terhune, M. Nisenhoff, and C. M. Savage, Phys. Rev. Lett. 8, 21 (1962).

[31]B. O. Seraphin and H. E. Bennett, *Semiconductors and Semimetals*, (Academic, New York, 1967), Vol. III.

[32]*American Institute of Physics Handbook*, 2nd Ed., edited by D. E. Grey (McGraw-Hill, New York, 1963).

[33]R. Bechman and S. Kurtz, in *Landolt-Börnstein Numerical Data and Functional Relationships*, edited by K. H. Hellwege and A. M. Hellwege (Springer-Verlag, Berlin, 1969), Vol. 2.

[34]M. Cardona, K. L. Shaklee, and F. H. Pollak, Phys. Rev. 154, 696 (1967).

[35]R. R. L. Zucca and Y. R. Shen, Phys. Rev. B 1, 2668 (1970).

[36]H. Ehrenreich, H. R. Phillipp, and J. C. Phillips, Phys. Rev. Lett. 8, 59 (1962). J. P. Walter, R. R. L. Zucca, M. L. Cohen, and Y. R. Shen, Phys. Rev. Lett. 24, 102 (1970).